nature photonics

ARTICLES

PUBLISHED ONLINE: 19 JANUARY 2015 | DOI: 10.1038/NPHOTON.2014.320

Deep-ultraviolet to mid-infrared supercontinuum generated in solid-core ZBLAN photonic crystal fibre

Xin Jiang[1]*, Nicolas Y. Joly[1,2], Martin A. Finger[1], Fehim Babic[1], Gordon K. L. Wong[1], John C. Travers[1] and Philip St. J. Russell[1,2]

Silica-based photonic crystal fibre has proven highly successful for supercontinuum generation, with smooth and flat spectral power densities. However, fused silica glass suffers from strong material absorption in the mid-infrared (>2,500 nm), as well as ultraviolet-related optical damage (solarization), which limits performance and lifetime in the ultraviolet (<380 nm). Supercontinuum generation in silica photonic crystal fibre is therefore only possible between these limits. A number of alternative glasses have been used to extend the mid-infrared performance, including chalcogenides, fluorides and heavy-metal oxides, but none has extended the ultraviolet performance. Here, we describe the successful fabrication (using the stack-and-draw technique) of a ZBLAN photonic crystal fibre with a high air-filling fraction, a small solid core, nanoscale features and near-perfect structure. We also report its use in the generation of ultrabroadband, long-term stable, supercontinua spanning more than three octaves in the spectral range 200–2,500 nm.

The physics of supercontinuum generation, having been studied for more than four decades[1], is now well understood. Detailed studies of nonlinear dynamics in optical fibres have led to several breakthroughs in extending and improving the quality of supercontinuum light sources[2]. The central role of the group velocity dispersion in controlling these dynamics means that solid-core silica–air photonic crystal fibre (PCF), the dispersion properties of which can be extensively engineered by varying the microstructure[3], has become the dominant medium not only for supercontinuum generation[4], but arguably for nonlinear fibre optics in general[5].

The main limitations of current solid-core PCF-based supercontinuum sources are material absorption (which in fused-silica glass climbs rapidly in the infrared, limiting spectral broadening to wavelengths below 2.5 μm) and solarization (which reduces the lifetime of silica fibres operating with wavelengths less than ~380 nm)[6]. For example, although Stark and colleagues reported supercontinuum generation down to a record 280 nm in a tapered silica solid-core PCF[7], ultraviolet-generated defect centres in the glass caused the performance to degrade after even short periods of operation. For these reasons, stable long-term deep-ultraviolet supercontinuum generation has not yet been successfully demonstrated in solid-core silica PCF.

Among the existing non-silica glasses, zirconium fluoride-based ($ZrF_4 > 50$ mol%) ZBLAN (ZrF_4–BaF_2–LaF_3–AlF_3–NaF) glass is transparent from 0.2 to 7.8 μm (see, for example, Fig. 1f) and has been viewed as an attractive material for optical devices from the deep-ultraviolet to the mid-infrared[8,9]. Since its discovery in 1975[8], ZBLAN has been regarded as a promising replacement for fused silica in telecommunications, suggesting that data transmission could be shifted to longer wavelengths where its attenuation is intrinsically much lower (less than 0.01 dB km^{-1} at 2.5 μm) than in fused silica (0.185 dB km^{-1} at 1.55 μm)[9,10]. Lack of effective methods for eliminating impurities (such as transition metals, oxy-fluorides and water), together with a steep viscosity–temperature characteristic, have made the drawing of high-quality ZBLAN fibres very difficult[9], even for conventional step-index structures. Nevertheless, it is also believed that, if carefully synthesized, ZBLAN glass can have extremely low water absorption, unlike common heavy-metal oxide or chalcogenide glasses[11], making it ideal for the generation of multi-octave-wide supercontinua over its entire transmission window.

Previous ZBLAN glass fibres have mainly been restricted to all-solid step-index geometries. The narrow temperature range (<10 °C, compared to ~300 °C for silica) over which the glass has suitable viscosity and is stable against devitrification[12,13] has created the perception that the drawing of ZBLAN microstructured fibres is extremely difficult, if not impossible. Yet another difficulty is low heat-transfer efficiency; because ZBLAN glasses are transparent in the infrared, radiative heat transfer over small distances from a heating element to the fibre preform is inefficient[9]. In addition, the thermal conductivity of ZBLAN is much lower than that of silica, so a specially designed drawing furnace must be used[9]. The only previous work on microstructured ZBLAN fibre used extrusion to produce a structure with a large (~100 μm) core surrounded by one ring of hollow channels[14].

Before the present work, ZBLAN-based supercontinuum spectra have been generated only in step-index fibres over the wavelength range from the visible to the mid-infrared, at very high powers[15–19]. No significant conversion to visible or ultraviolet wavelengths has been possible, however, because of the unsuitable dispersion of these large-core all-solid fibres, whose relatively low effective nonlinearity makes it necessary to use long fibre lengths, further limiting the transmission window to the range 300 nm to 4.5 μm (ref. 20). Further broadening into the mid-infrared region from 1.4 to 13.3 μm has recently been achieved using mid-infrared laser pulses at 6.3 μm and a large-core step-index As_2Se_3 chalcogenide glass fibre[21].

In this Article, we describe a simple supercontinuum system based on a 4-cm-long, small-solid-core ZBLAN PCF with high axial uniformity. By controlling the dispersion through appropriate fibre design we generate several supercontinuum spectra, some of which extend down to 200 nm and others up to 2,500 nm, using a relatively low power and compact laser operating at 1,042 nm. The

[1]Max Planck Institute for the Science of Light, Guenther-Scharowsky Strasse 1, Bau 24, Erlangen 91058, Germany. [2]Department of Physics, University of Erlangen-Nuremberg, Guenther-Scharowsky Strasse 1, Bau 24, Erlangen 91058, Germany. *e-mail: xin.jiang@mpl.mpg.de

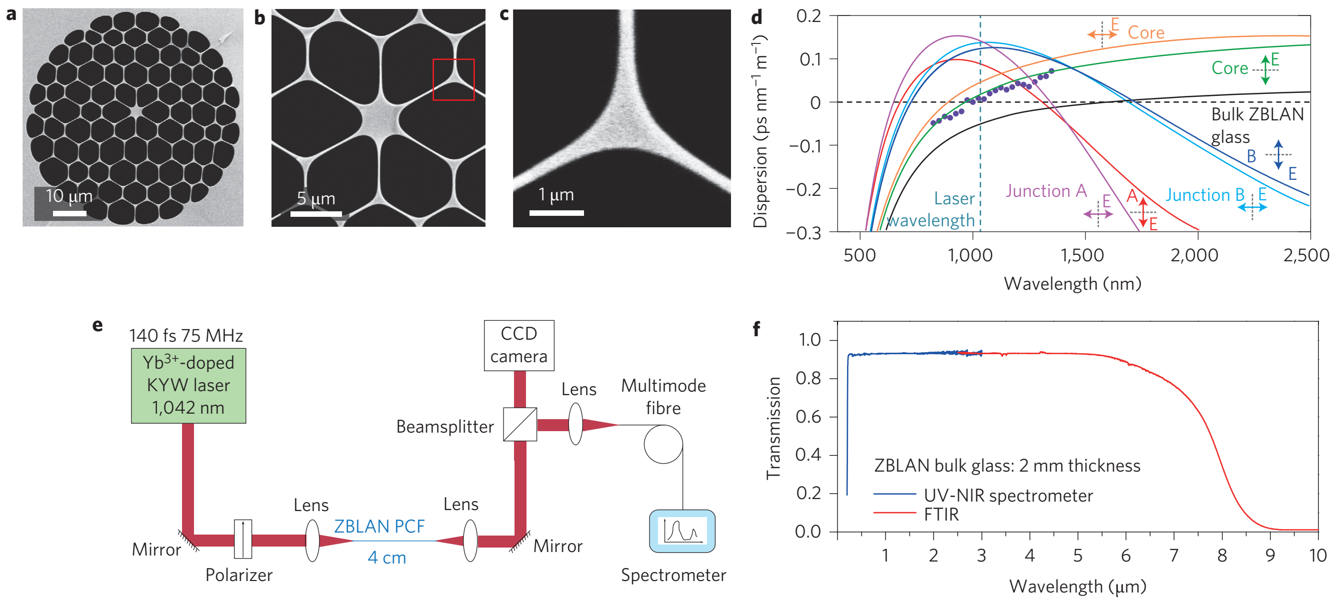

Figure 1 | Measured and calculated ZBLAN PCF parameters and experimental set-up for supercontinuum generation. a–c, SEM images of the cross-section of the ZBLAN PCF. The triangular cladding interstices have a diameter of ~1 μm, and can be used for supercontinuum generation (see main text). **d**, Calculated wavelength-dependent dispersion of the modes of the core and two different interstitial junctions in the cladding. The dispersion of the bulk glass and of the two orthogonally polarized modes of the fibre core (junctions A and B) are plotted. Purple dots are data points measured using low-coherence interferometry for light polarized along the long axis of the core. **e**, Experimental set-up for supercontinuum generation in a highly nonlinear ZBLAN PCF (see Methods). CCD, charge-coupled device. **f**, Transmission spectrum of a ZBLAN bulk glass sample (~2 mm thick), polished on both sides and measured using an ultraviolet–near-infrared (UV–NIR) spectrometer and a Fourier-transform infrared (FTIR) spectrometer.

over three-octave-wide supercontinua have high brightness and spectral flatness and, remarkably, the fibres show no sign of degradation as a result of ultraviolet-induced solarization. Deep-ultraviolet supercontinuum generation has not been seen before in any solid-core optical fibre. Indeed, such short wavelengths have only previously been obtained in gas-filled hollow-core PCFs, requiring few-microjoule femtosecond pump pulses from large and complex laser systems[22,23].

Fibre properties and experimental implementation

Figure 1a–c presents scanning electron microscopy (SEM) images of the cross-section of the ZBLAN-PCF (for fabrication techniques see Methods). The core is slightly elliptical with an average diameter of ~3 μm, and is surrounded by five rows of hollow cladding channels interspersed with triangular interstitial junctions with a diameter of ~1 μm (Fig. 1c). The glass webs connecting adjacent interstices are ~150 nm wide, the pitch between cladding holes is 4.3 μm, and the air-filling fraction of the cladding structure is ~88%. As can be seen in Fig. 1b,c, the interstitial junctions in the cladding are optically quite isolated from one another (see, for example, the red square), permitting their use as independent guiding cores (at least at shorter wavelengths, when the modal fields remain localized)[24].

The measured dispersion of one of the linearly polarized modes of the core is presented in Fig. 1d (dark purple dots), together with the results of numerical modelling (see Methods) for both the fibre modes and bulk glass material, which has a zero dispersion wavelength (ZDW) at 1.62 μm. The interstitial junctions are triangular and the fundamental modes in them are well confined to the glass at a wavelength of 1 μm (Fig. 2d, inset), although they spread out more at longer wavelengths.

Supercontinua spanning at least one octave were generated when pulses were launched into the fibre core (Supplementary Section 1). In contrast, when light was launched into individual interstitial junctions in the cladding, many produced supercontinua over three octaves wide. Here, we consider two interstitial junctions, each selected from a different length of fibre. Junction A is from the outermost ring of the first fibre and junction B lies between the second and third rings of the second fibre. The strong waveguide dispersion induced by tight modal confinement in these junctions causes them both to have two ZDWs. Both junctions are birefringent, as indicated in Fig. 1d, where the calculated dispersion of the two orthogonally polarized modes of junctions A and B is plotted. Along one polarized mode, junction A has ZDWs at 670 and 1,300 nm, whereas junction B has ZDWs at 700 and 1,720 nm.

Figure 1f presents the transmission of the ZBLAN glass used to make the fibre. The ultraviolet absorption edge is at ~200 nm, whereas in the infrared, transmission is possible beyond 6 μm. Between 200 nm and 6 μm the glass offers a flat window of transmission, ideal for multi-octave-wide supercontinuum generation, with no evidence of absorption caused by contamination with OH^- or transition metals, nor any evidence of scattering by microcrystallites or glass defects such as bubbles, grain boundaries, and so on.

Figure 1e presents the experimental set-up. The pump laser emitted pulses of duration 140 fs at 1,042 nm with 75 MHz repetition rate (for full details see Methods). Pumping junction A with 830 pJ of launched pulse energy resulted in the generation of a supercontinuum greater than three octaves wide, extending from 200 nm to 1,750 nm, as shown in Fig. 2a. The deep- to near-ultraviolet (200–400 nm) contains over 10% of the total power in the supercontinuum (Fig. 3), and was readily observable without sensitive optimization of the spectrometers. The measured near-field mode profiles at several different wavelengths from the deep-ultraviolet to near-infrared are presented in Fig. 2b, showing that the emission is in the fundamental mode. Figure 2c presents a zoom-in of the ultraviolet region inside the dotted square in Fig. 2a, replotted against frequency with a linear vertical scale. The spectrum is clearly multipeaked. The inset photograph in Fig. 2c shows the light emitted by the fibre, dispersed by a fused-silica

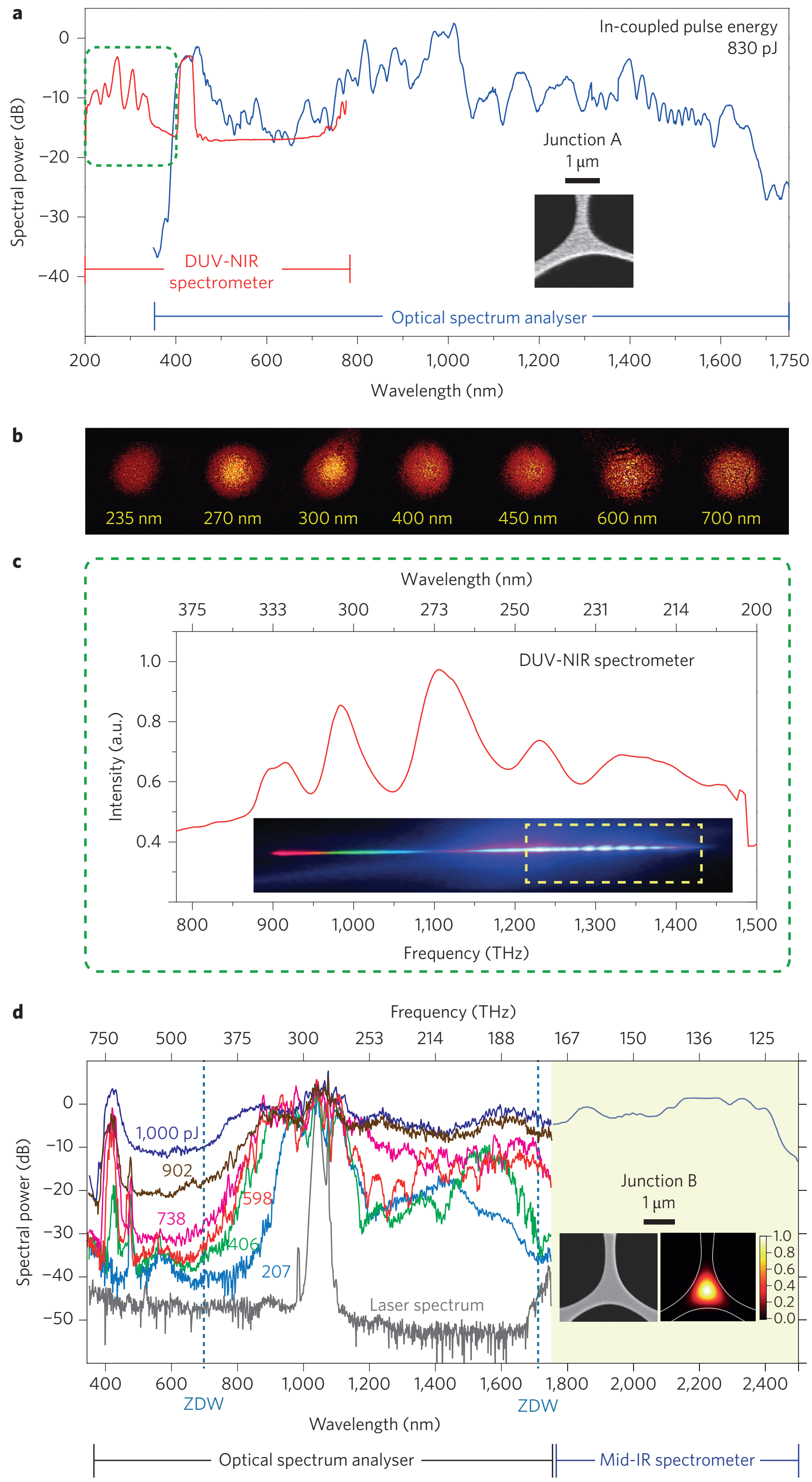

Figure 2 | Experimental supercontinuum generation in junctions A and B. a, Supercontinuum spectrum generated by junction A for a launched pump energy of 830 pJ. Inset: SEM image of the junction. DUV, deep-ultraviolet; NIR, near-infrared. **b**, Near-field mode profiles measured after transmission through bandpass filters. **c**, Magnified plot of the ultraviolet section of the supercontinuum spectrum (dotted square in **a**), replotted against frequency with a linear vertical scale. Inset: photograph showing the spectrum after being dispersed by a fused-silica prism and cast onto a white screen (see main text). **d**, Spectral broadening by junction B at successively higher launched pulse energies up to 1 nJ. Grey curve, laser spectrum. Inset: SEM image of the junction and calculated mode intensity profile at 1,000 nm (from finite-element simulations).

prism and cast onto a white screen. The colour varies smoothly from red to blue, after which an extended blue-white band is seen, which is the result of ultraviolet-induced photoluminescence of the screen (within the dotted yellow rectangle). Within this region the multi-peaked nature of the spectrum is clearly seen, in agreement with the measured spectrum in Fig. 2c.

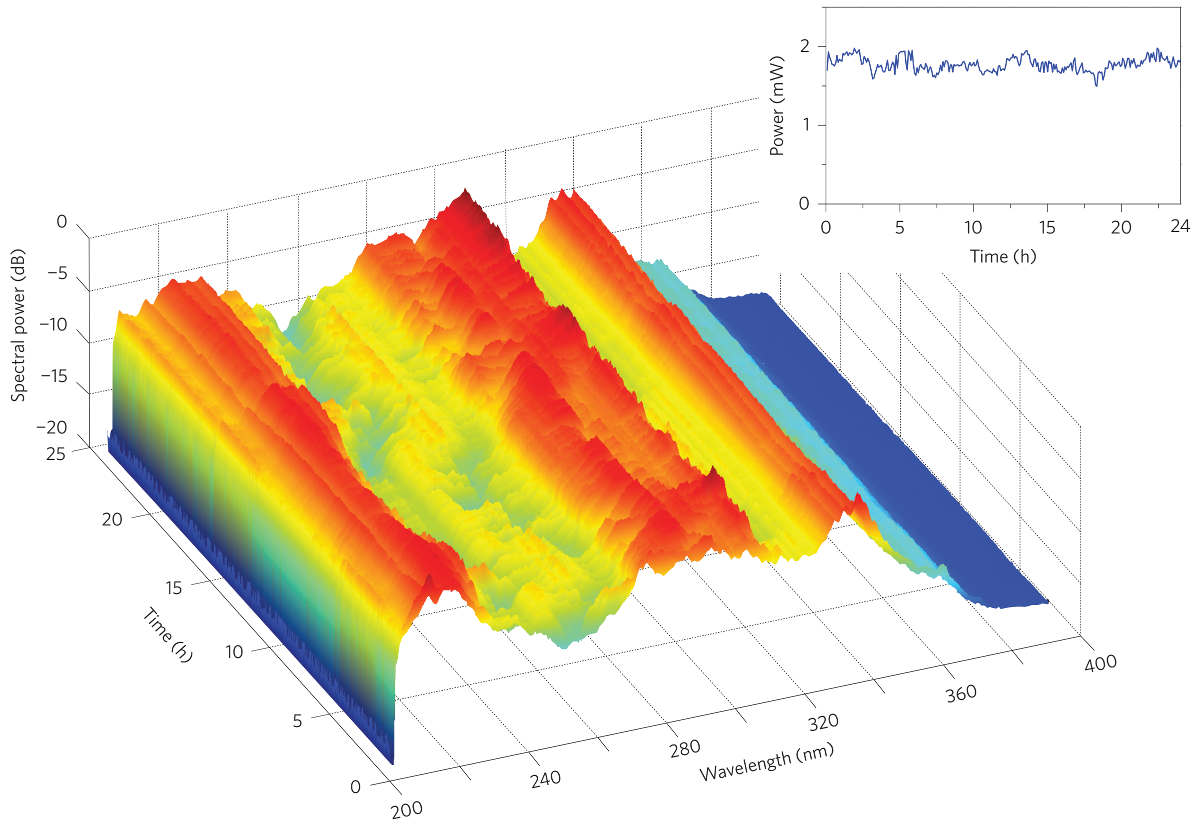

Figure 3 | Long-term stability during continuous ultraviolet supercontinuum generation from 200 to 400 nm. Spectra were recorded by an ultraviolet spectrometer, programmed to record every 5 min over a period of 24 h. Inset: integrated output power between 200 and 400 nm, plotted as a function of time (see Methods for power calibration). It remains constant at ~2 mW, which corresponds to more than 10% of the total power in the supercontinuum.

Figure 2d presents the results of pumping interstitial junction B with the maximum available energy (~1 nJ launched into the mode). The supercontinuum spectrum extends from ~400 to 2,500 nm with a flatness better than 10 dB, and from 800 nm to 2.4 μm with a flatness better than 3 dB. The average spectral energy density is ~0.47 pJ nm^{-1} over this range.

Lifetime stability of ultraviolet light generation

The ultraviolet light emission from junction A showed no signs of optical damage, even after running experiments for 5–6 h every day over a period of a few months. This was further verified by performing lifetime experiments in which the spectrum between 200 and 400 nm was recorded at 5 min intervals over 24 h. Figure 3 presents one set of measurements (for more results see Supplementary Section 2). There is no sign of degradation, which is remarkable given the high spectral power and short wavelength of the ultraviolet emission, which would rapidly damage a silica glass core. The slight variations in the spectrum we attribute to mechanical drift in the launching stages and perturbations due to vibrations from nearby devices.

Discussion

The nonlinear dynamics in the visible and near-infrared can mostly be understood by reference to conventional nonlinear processes. Figure 4a presents detailed measurements of the formation and evolution of the short-wavelength spectrum emitted from junction A as a function of pump energy, and Fig. 4b shows the results of comparative numerical simulations. The agreement is very good (see Methods for details). The different stages of spectral evolution are annotated (i) to (vi) in Fig. 4 and in companion XFROG spectrograms in Supplementary Fig. 4. Both junction A and junction B are pumped in the anomalous dispersion region between two ZDWs, a regime that has been widely studied[24–26]. As the pump energy is increased it is clear, from the characteristic symmetric broadening of the pump laser in Fig. 4a,b (i), that the pulse undergoes increasing soliton-effect self-compression. After sufficient spectral broadening and temporal compression, soliton fission occurs[27] due to the close-lying dispersion zeros. In junction B the solitons undergo a Raman-driven self-frequency redshift up to the second ZDW at 1,720 nm, forming a soliton-Raman continuum (not shown), and when these solitons reach the second ZDW they emit a long-wavelength dispersive wave[28]. This process is what forms the broad infrared supercontinuum shown in the experimental spectra of Fig. 2d. In contrast, for junction A, the closer vicinity of the second ZDW (1,300 nm) prohibits this effect. Instead, the solitons remain close to the pump wavelength, and dispersive radiation is emitted into the normal dispersion regions (Fig. 4a,b, ii). At higher energy, dispersive radiation can be generated simultaneously on both the short- and long-wavelength edges, as previously observed in silica fibres[24–26]. The spectral recoil from the emission of the long-wavelength dispersive wave leads to a predominant blueshift of the soliton spectrum, which is clearly visible in both the experimental spectra and the numerical simulations in Fig. 4a,b (iii), where the upshifted spectrum extends to below 800 nm, still in the anomalous dispersion region. It is also clear from the spectral interference fringes in Fig. 4a,b (iii) that multiple solitons undergo a blueshift. This is further evidenced by the blueshifted solitons in Supplementary Fig. 4d (iii). At these energies, the blueshifted solitons are approaching the short-wavelength ZDW and emit an enhanced short-wavelength dispersive wave at 400–500 nm, as shown at Fig. 4 (iv), in agreement with phase-matching calculations. At yet higher pump energies, more solitons are created, and mixing between them and dispersive waves[29] leads to a filling-in of the supercontinuum. Supplementary Fig. 4e shows that at 1 nJ the simulated supercontinuum spectrum extends out to 2,500 nm and

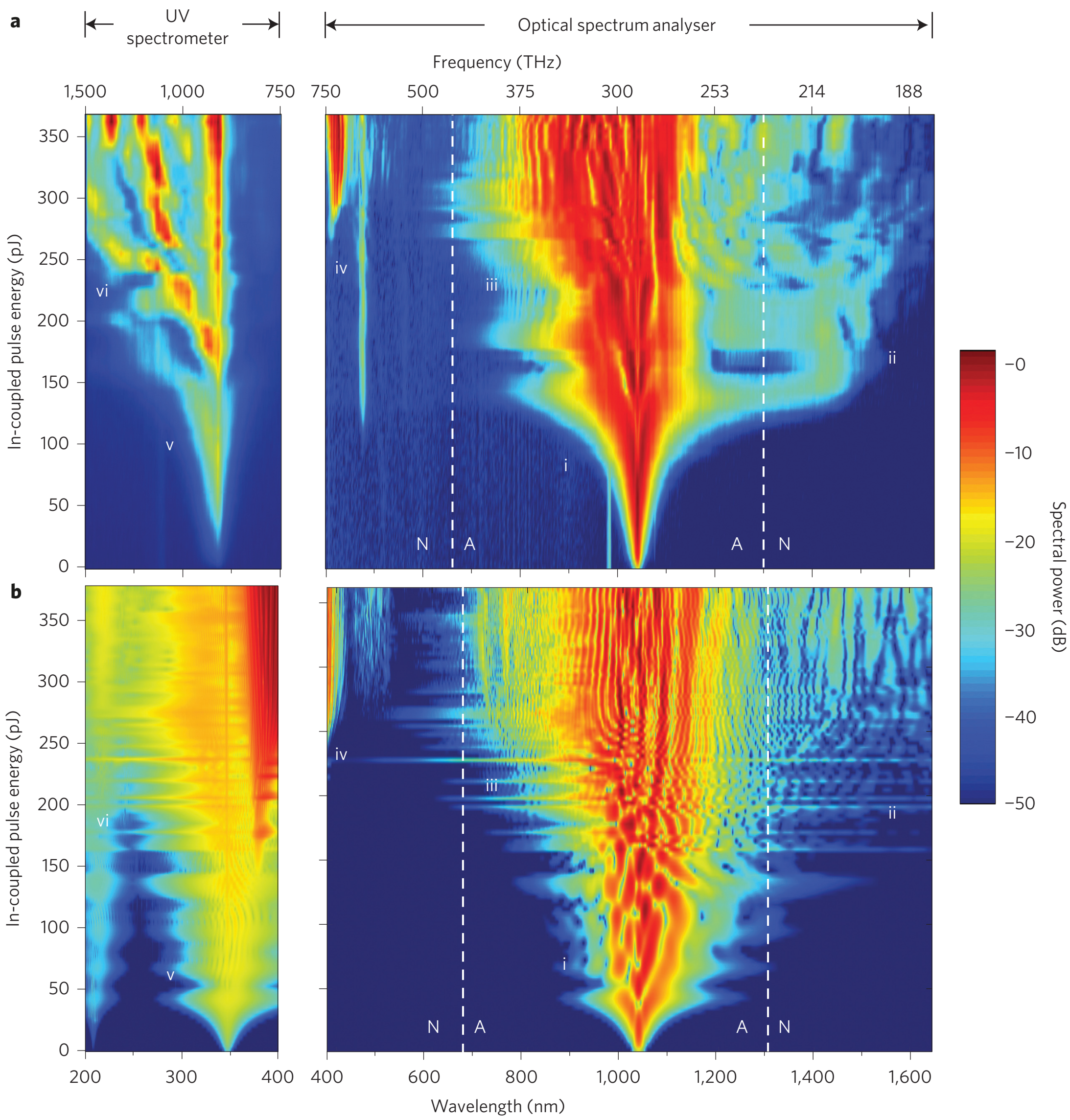

Figure 4 | Measured and simulated supercontinuum generation in junction A. a, Energy dependence of ultraviolet and visible–near-infrared spectra generated by junction A of a 4-cm-long fibre, measured for launched pulse energies from 3 to 362 pJ. Measured data from the ultraviolet spectrometer and optical spectrum analyser were first normalized and then plotted on a logarithmic scale. **b**, Numerically simulated energy dependence for the same conditions. Roman numerals are as described in Supplementary Section 2. A and N: anomalous and normal dispersion regions. Note that both the experimental and numerical ultraviolet plots are on an enhanced colour density scale. The bright horizontal spectral features in **b** are real and correspond to soliton collisions not resolved in the experiments.

the overall supercontinuum shape and extent in the visible and infrared regions agree quite well with the experimental results in Fig. 2. The long-wavelength cutoff is caused by a combination of the second ZDW, which limits the soliton redshift, and the small junction size, which causes the optical modes to spread out at longer wavelengths, reducing the effective nonlinearity and increasing confinement loss. For optimal long-wavelength supercontinua the fibre should be redesigned so as to display no second (long-wavelength) ZDW.

The origin of the deep-ultraviolet emission is less easy to explain. It appears that strong third-harmonic generation (THG), starting at the lowest pump energy and clearly visible in Fig. 4a,b (v), is mostly responsible. In particular, note how the blue-edge of the deep-ultraviolet spectrum mirrors the blue-edge of the spectrum around the pump, at approximately one-third of the wavelength (compare regions (iii) and (vi) in Fig. 4a,b). We therefore suggest that the blueshift in the deep-ultraviolet is caused by THG and cross-phase modulation from the blueshifting solitons. The numerical simulations clearly show some ultraviolet generation, including the similarities between regions (iii) and (vi); however, the brightness and internal spectral multipeak structure of the deep-ultraviolet band are unexpected and not reproduced. Understanding the origin of this emission is also complicated by a lack of knowledge of the material parameters in this region. The Sellmeier fits used for the material dispersion were determined from measurements down to only 405 nm. Additionally, when operating so close to the electronic band-edge (which we estimate to lie at ~5.8 eV, that is, 214 nm), the empirical Sellmeier expansion will become invalid[30] and the estimated values of dispersion inaccurate. The nonlinear properties will also be strongly modified[31], and the creation of free carriers due to multiphoton absorption cannot be ruled out. From best estimates of the dispersion, neither THG nor dispersive-wave emission, nor indeed any of the plethora of four-wave mixing processes (both conventional and intra-soliton[29]), are phase-matched in this region, even when we include higher-order modes (note the experimental evidence in Fig. 2b indicating that emission is in the fundamental mode). This may indicate that the dispersion deviates strongly from the Sellmeier approximation in the deep-ultraviolet. In the absence of relevant data, we leave a full explanation of the origin and strength of the experimentally measured ultraviolet emission as an open question.

In conclusion, PCFs with large air-filling fractions, sub-micrometre-scale features and unprecedented axial uniformity can be drawn from ZBLAN glass—something previously regarded as unfeasible. The ability to strongly modify the dispersion landscape using PCF designs represents a significant advance compared to previous work based on all-solid step-index ZBLAN fibres. Given that the glass is transparent from the deep-ultraviolet to mid-infrared, this opens up new possibilities for the generation of ultra-broadband supercontinua in a simple system, with applications in, for example, ultraviolet and infrared spectroscopy and metrology. The high spectral power of the deep-ultraviolet emission and the remarkable lack of material damage is particularly striking. We are currently limited by the availability of the ZBLAN glass, so, although we are confident that we can make ZBLAN fibres with a smaller central core (making the use of cladding nodes unnecessary), this has so far not been possible. In future work we plan to explore simplified fibre structures, such as suspended core 'Mercedes' fibres and PCFs with dispersion curves optimized for infrared supercontinuum generation. Finally, ZBLAN is also an excellent host for rare-earth ions, suggesting the possibility of ultra-broadband intracavity supercontinuum generation in fibre lasers.

Methods

Fibre fabrication and characterization. The stack-and-draw technique is well proven as a most suitable and flexible method for fabricating various types of PCF from fused silica. For PCFs made from soft glasses, however, techniques such as extrusion and etching have also been used[32,33]. By careful optimization of the multistep stack-and-draw procedure, we recently reported an enhanced drawing procedure that allowed the fabrication from Schott SF6 glass of a highly uniform, kagomé-like hollow-core fibre structure that offered effectively single-mode guidance[34]. Here, we report further improvements to this technique, eliminating structural distortion and allowing the fabrication of small-core PCFs from ZBLAN glass. A customized heating element was used to provide a uniform heating around the preform. This element provided a long preheating zone of ~100 mm with a slow ramping profile and a short hot zone less than 10 mm long, offering temperature fluctuations as small as ±0.5 °C. After the hot zone, the temperature dropped extremely quickly. ZBLAN glass is extremely hydroscopic, which means, if heated, it can easily absorb moisture in air, degrade and crystallize (microcrystallites in the glass will create scattering centres). As a result, it is essential that the ZBLAN PCF is drawn in an inert atmosphere. The inner chamber of the drawing furnace was therefore purged with argon gas at a rate of ~7 l min^{-1}. Handling of the fibre preform (storage, preparation and fibre drawing) was carefully managed so as to exclude potential contact with water or humid air. The drawing temperature was precisely controlled to between 308 and 313 °C, corresponding to a glass viscosity range from $10^{6.0}$ to $10^{5.4}$ Pa s. During drawing we used a relatively fast preform feeding rate of 5–10 mm min^{-1} to decrease the dwell time of the preform in the hot zone and thus reduce the risk of crystallization. The endface of the fibre preform was connected to a pressure unit and continuously pumped with dry nitrogen gas so as to control the fibre structure. The core/junction size and air-filling fraction were controlled by changing the feeding/pulling rates and the hole pressure during drawing.

The dispersion of the core mode was measured using conventional low-coherence interferometry[35]. The numerically calculated dispersion curves were obtained using finite-element calculations (JCMwave) on the actual fibre structures extracted from high-resolution SEM images and surrounded by transparent boundary conditions. The effective areas of the junctions were calculated using the full vectorial method of ref. 36 from the finite element method (FEM) results.

Supercontinuum experiments. An Yb^{3+}-doped potassium-yttrium-tungstate (KYW) laser delivering 140 fs pulses with 75 MHz repetition rate at a wavelength of 1,042 nm was used as the pump source. The maximum available energy was 11.8 nJ. The pulses were launched into a 4-cm-long ZBLAN PCF using free-space optics with mirrors and lenses. Because the waveguides are typically form-birefringent, a linear polarizer was placed before the fibre to allow launching into a single eigenmode. FROG measurements confirmed that the launched pulses were transform-limited; that is, the precoupling optics did not significantly affect the pulse characteristics. By tightly focusing the laser light and scanning across the cladding structure so as to visit different interstitial junctions one by one, we were able to select junctions that yielded the highest launch efficiency and the broadest supercontinuum. A coupling efficiency of 6–8% into the junctions was achieved.

Three spectrometers were used to analyse the supercontinuum: an ultraviolet–visible spectrometer (Ocean Optics Maya 2,000 Pro, 200–750 nm), an optical spectrum analyser (Yokogawa AQ6315A, 350–1,750 nm) and an infrared spectrometer (Ocean Optics NIR quest, 1,750–2,500 nm). An ultraviolet–visible charge-coupled device camera beam profiler (Thorlabs BC106N-UV/BC106N-Vis) was used to measure the near-field mode profiles.

The lower bound of the spectral power in the ultraviolet was determined by blocking the prism-dispersed supercontinuum light at wavelengths longer than 400 nm, and the remainder was measured with a thermal power meter.

Numerical simulations. Numerical simulations were performed using a unidirectional full field equation including the Kerr and Raman effects and THG[37,38].

The reported values for the nonlinear refractive index of ZBLAN vary from 2.1×10^{-16} $\mathrm{cm^2\,W^{-1}}$ (ref. 19) to 5.4×10^{-16} $\mathrm{cm^2\,W^{-1}}$ (ref. 39). We used a value of 5.4×10^{-16} $\mathrm{cm^2\,W^{-1}}$, which reproduced the relatively narrow spectral broadening (0.6–1.55 μm) observed when light was launched into the 3 μm central core.

The Raman contribution for ZBLAN is commonly described as a single Lorentzian[40], but a more complex description has recently been developed that provides a better fit to the overall shape of the Raman gain spectrum[39]. An accurate value for the peak Raman gain is also important. Values in the literature range from $4.0 \pm 2 \times 10^{-14}$ $\mathrm{m\,W^{-1}}$ to $2.0 \pm 0.5 \times 10^{-13}$ $\mathrm{m\,W^{-1}}$ (ref. 19), compared to 6×10^{-15} $\mathrm{m\,W^{-1}}$ in silica[39]. In the simulations we used the Raman gain spectrum reported by Yan and co-authors[39].

Received 10 August 2014; accepted 2 December 2014; published online 19 January 2015

References

1. Alfano, R. R. & Shapiro, S. L. Observation of self-phase modulation and small-scale filaments in crystals and glasses. *Phys. Rev. Lett.* **24,** 592–594 (1970).
2. Dudley, J. M. & Taylor, J. R. *Supercontinuum Generation in Optical Fibers* (Cambridge Univ. Press, 2010).
3. Russell, P. St. J. Photonic-crystal fibres. *J. Lightwave Technol.* **24,** 4729–4749 (2006).
4. Dudley, J. M., Genty, G. & Coen, S. Supercontinuum generation in photonic crystal fiber. *Rev. Mod. Phys.* **78,** 1135–1184 (2006).
5. Dudley, J. M. & Taylor, J. R. Ten years of nonlinear optics in photonic crystal fibre. *Nature Photon.* **3,** 85–90 (2009).
6. Bach, H. & Neuroth, N. *The Properties of Optical Glasses* (Springer-Verlag, 1995).
7. Stark, S. P., Travers, J. C., Russell, P. St. J. Extreme supercontinuum generation to the deep UV. *Opt. Lett.* **37,** 770–772 (2012).
8. Gan, F. Optical properties of fluoride glasses: a review. *J. Non-Cryst. Solids* **184,** 9–203 (1995).
9. Cable, M. & Parker, J. M. *High-Performance Glasses* (Chapman and Hall, 1992).
10. Hill, G. *The Cable and Telecommunications Professionals' Reference: Transport Networks* (Focal Press, Elsevier, 2008).
11. Harrington, J. A. *Infrared Fibers and their Applications* (SPIE, The International Society for Optical Engineering, 2004).
12. Aasland, S. & Grande, T. Crystallization of ZBLAN glass. *J. Am. Ceram. Soc.* **79,** 2205–22063 (1996).
13. Smektala, F. & Matecki, M. Stability study on heating and determination of critical cooling rates of fluorozirconate glasses. *J. Non-Cryst. Solids* **184,** 314–3183 (1995).
14. Ebendorff-Heidepriem, H. *et al.* Fluoride glass microstructured optical fiber with large mode area and mid-infrared transmission. *Opt. Lett.* **33,** 2861–2863 (2008).
15. Xia, C. *et al.* Mid-infrared supercontinuum generation to 4.5 μm in ZBLAN fluoride fibers by nanosecond diode pumping. *Opt. Lett.* **31,** 2553–2555 (2006).
16. Qin, G. *et al.* Ultrabroadband supercontinuum generation from ultraviolet to 6.28 μm in a fluoride fiber. *App. Phys. Lett.* **95,** 161103 (2009).
17. Heidt, A. M. *et al.* Mid-infrared ZBLAN fiber supercontinuum source using picosecond diode-pumping at 2 μm. *Opt. Express* **21,** 24281–24287 (2013).
18. Yang, W., Zhang, B., Yin, K., Zhou, X. & Hou, J. High power all fiber mid-IR supercontinuum generation in a ZBLAN fiber pumped by a 2 μm MOPA system. *Opt. Express* **21,** 19732–19742 (2013).
19. Agger, C. *et al.* Supercontinuum generation in ZBLAN fibers—detailed comparison between measurement and simulation. *J. Opt. Soc. Am. B* **29,** 635–645 (2012).
20. Saad, M. Fluoride glass fiber: state of the art. *Proc. SPIE* **7316,** 7316N1–N16 (2009).
21. Petersen, C. R. *et al.* Mid-infrared supercontinuum covering the 1.4–13.3 μm molecular fingerprint region using ultra-high NA chalcogenide step-index fibre. *Nature Photon.* **8,** 830–834 (2014).
22. Joly, N. Y. *et al.* Bright spatially coherent wavelength-tunable deep-UV laser source using an Ar-filled photonic crystal fiber. *Phys. Rev. Lett.* **106,** 203901 (2011).

23. Mak, K. F., Travers, J. C., Hölzer, P., Joly, N. Y. & Russell, P. St. J. Tunable vacuum-UV to visible ultrafast pulse source based on gas-filled Kagome-PCF. *Opt. Express* **21,** 10942–10953 (2013).
24. Benabid, F. *et al.* Fourth-order dispersion mediated solitonic radiations in HC-PCF cladding. *Opt. Lett.* **33,** 2680–2682 (2008).
25. Hilligsøe, K. M. *et al.* Supercontinuum generation in a photonic crystal fiber with two zero dispersion wavelengths. *Opt. Express* **12,** 1045–1054 (2004).
26. Birks, T. A., Wadsworth, W. J. & Russell, P. St. J. Supercontinuum generation in tapered fibers. *Opt. Lett.* **25,** 1415–1417 (2000).
27. Husakou, A. V. & Herrmann, J. Supercontinuum generation of higher-order solitons by fission in photonic crystal fibers. *Phys. Rev. Lett.* **87,** 203901 (2001).
28. Skryabin, D. V., Luan, F., Knight, J. C. & Russell, P. St. J. Soliton self-frequency shift cancellation in photonic crystal fibers. *Science* **301,** 1705–1708 (2003).
29. Skryabin, D. V. & Yulin, A. V. Theory of generation of new frequencies by mixing of solitons and dispersive waves in optical fibers. *Phys. Rev. E* **72,** 016619 (2005).
30. Marcuse, D. *Light Transmission Optics* (Van Nostrand-Reinhold, 1982).
31. DeSalvo, R., Said, A. A., Hagan, D. J., Stryland, E. W. V. & Sheik-Bahae, M. Infrared to ultraviolet measurements of two-photon absorption and N_2 in wide bandgap solids. *IEEE J. Quantum Electron.* **32,** 1324–1333 (1996).
32. Ebendorff-Heidepriem, H. & Monro, T. M. Extrusion of complex preforms for microstructured optical fibers. *Opt. Express* **15,** 15086–15092 (2007).
33. Coulombier, Q. *et al.* Casting method for producing low-loss chalcogenide microstructured optical fibers. *Opt. Express* **18,** 9107–9112 (2010).
34. Jiang, X. *et al.* Single-mode hollow-core photonic crystal fiber made from soft glass. *Opt. Express* **19,** 15438–15444 (2011).
35. Shang, H. Chromatic dispersion measurement by white-light interferometry on metre-length single-mode optical fibres. *Electron. Lett.* **17,** 603–605 (1981).
36. Tzolov, V. P., Fontaine, M., Godbout, N. & Lacroix, S. Nonlinear self-phase-modulation effects: a vectorial first-order perturbation approach. *Opt. Lett.* **20,** 456–458 (1995).
37. Tani, F., Travers, J. C. & Russell, P. St. J. Multimode ultrafast nonlinear optics in optical waveguides: numerical modelling and experiments in Kagomé photonic-crystal fiber. *J. Opt. Soc. Am. B* **31,** 311–320 (2014).
38. Kolesik, M. & Moloney, J. V. Nonlinear optical pulse propagation simulation: from Maxwell's to unidirectional equations. *Phys. Rev. E* **70,** 036604 (2004).
39. Yan, X. *et al.* Raman transient response and enhanced soliton self-frequency shift in ZBLAN fiber. *J. Opt. Soc. Am. B* **29,** 238–243 (2012).
40. Petersen, C. *et al.* Stimulated Raman scattering in soft glass fluoride fibers. *J. Opt. Soc. Am. B* **28,** 2310–2313 (2011).

Acknowledgements
The ZBLAN glass rods and tubes were purchased from IRphotonics (now part of Thorlabs).

Author contributions
X.J. and F.B. designed, fabricated and characterized the fibre. X.J. and N.Y.J. carried out the experiments on supercontinuum generation. J.C.T. performed the majority of the theoretical analysis and numerical simulations. P.St.J.R. conceived the project and supervised the work. M.A.F. and G.K.L.W. assisted the work in various ways.

Additional information
Supplementary information is available in the online version of the paper. Reprints and permissions information is available online at www.nature.com/reprints. Correspondence and requests for materials should be addressed to X.J.

Competing financial interests
The authors declare no competing financial interests.